ILD-PHYS-PROC–2026-008
25 February 2026

# $e^+e^- \to s\bar{s}$ at $\sqrt{s} = 250$ GeV in future linear colliders

J.P. Márquez[1] [1)], R. Pöschl[1]

[1] *IJCLab, CNRS & U. Paris-Saclay, 15 rue Georges Clémenceau, Orsay, 91400, France*

## Abstract

The forward–backward asymmetry ($A_{FB}$) in light-quark production is a sensitive probe of the electroweak sector and potential flavour-dependent BSM effects. We present a study of $e^+e^- \to s\bar{s}$ at $\sqrt{s} = 250$ GeV at future linear colliders, using full ILD simulation and reconstruction tools for ILC and LCF@CERN.

We assess the impact of particle identification on charge reconstruction and $A_{FB}$ extraction, considering software improvements using CPID for optimal $dE/dx$ usage, as well as hardware scenarios including cluster counting ($dN/dx$) and ideal TPC performance. Statistical precision gains are evaluated, with corrections for charge misidentification and acceptance applied.

Results indicate that precise $A_{FB}^{s\bar{s}}$ measurements are feasible and that advanced PID is key to maximising sensitivity to electroweak and new-physics effects.

*This work was carried out in the framework of the ILD concept group*
*Talk presented at the International Workshop on Future Linear Colliders (LCWS 2025), TBD*

[1)] Speaker jesus.marquez@ific.uv.es

# 1 Introduction

The study of quark pair production in $e^+e^-$ collisions provides a precise probe of electroweak interactions and is sensitive to the chiral structure of the SM, which would be modified by BSM contributions. This in turn would lead to measurable modulations of the differential cross section that impact the *Forward-Backward Asymmetry* ($A_{FB}$), defined as:

$$A_{FB}^{q\bar{q}} = \frac{\sigma^F - \sigma^B}{\sigma^F + \sigma^B}. \tag{1}$$

Here, $\sigma^{F/B}$ is the differential cross-section integrated over the forward/backward hemisphere. This work focuses on $e^+e^- \to s\bar{s}$ at $\sqrt{s} = 250$ GeV, comparing ILC250 [1–5] and LCF@CERN250 [6, 7]. Both feature polarised beams (80% $e^-$, 30% $e^+$) and foreseen integrated luminosities of 2 ab$^{-1}$ (ILC) and 3 ab$^{-1}$ (LCF). Four beam polarisation schemes are envisioned: P$(e^-,e^+)$=$(\pm0.8,\pm0.3)$. For simplicity, we denote $(+0.8,-0.3)$ as $e_L^-e_R^+$ and $(+0.8,+0.3)$ as $e_R^-e_L^+$. In this work, we consider only the $e_L^-e_R^+$ and $e_R^-e_L^+$ polarizations, each with 45% of the total integrated luminosity.

Following previous heavy-quark studies [8–15], we extend the analysis to strange-quark production [14, 16].

# 2 Methodology and results in the baseline $dE/dx$ analysis

## Preselection of $q\bar{q}$ events

The events are simulated (Refs. [17–20]) and reconstructed with the standard ILD chain (Refs.[21–23]), producing *Particle Flow Objects* (PFOs), jets and flavour-tagging information.

After reconstruction of the main physics objects (tracks, jets, PFOs, heavy quark tagging, and PID), an event preselection is applied using kinematic cuts to enrich the signal and reduce backgrounds. The backgrounds suppressed by this preselection arise from heavy boson pair production ($W^+W^-$, $ZH$, $ZZ$). The same set of cuts also mitigates the impact of radiative return events, which would otherwise dilute the measured cross section. The preselection at 250 GeV is as in Ref. [12]:

1. Photon veto cuts, rejecting events if:
   a) at least one jet contains only one PFO;
   b) at least one jet contains a reconstructed $\gamma_{\text{cluster}}$ with $E > 115$ GeV or located in the forward region $|\cos\theta| > 0.97$;
2. Events with $\sin\Psi_{\text{acol}} > 0.3$ are rejected;
3. Events with $m_{jj} < 140$ GeV are rejected;
4. Events with $y_{23} > 0.02$ are rejected.

## Strange tagging based on kaon PID

Until recently, no strange tagging algorithm was available. Therefore, a simple cut-based $s$-tagger was developed in Ref. [14]. The cut-flow of the $s$-tagging in this analysis is slightly different from that of the reference and is listed in Tab. 1.

The event selection cuts are grouped as follows: cuts 1–3 suppress heavy-quark backgrounds, 4–7 select s-jets via kaon PID, and 8–9 reduce migration effects.

Compared to the analysis in Ref. [14], the main modification concerns cut 7. A two-dimensional mapping of the PID observables is used to define a region identifying a PFO as a kaon. The track $dE/dx$

| # | Name | Quantity |
|---|---|---|
| 1 | b-tag | b-tag $< 0.3$ |
| 2 | c-tag | c-tag $< 0.65$ |
| 3 | nvtx | nvtx $= 1$ |
| 4 | LPFO momentum | $p_{\mathrm{LPFO}} > 15$ GeV |
| 5 | LPFO acollinearity | $\cos\theta_{\mathrm{LPFO}_{1,2}} > 0.95$ |
| 6 | Offset | $V_0 = \sqrt{d_0^2 + z_0^2} < 1$ mm |
| 7 | $dE/dx$ PID K | If $\lvert\cos\theta\rvert < 0.85$, $\lvert k_{\mathrm{dist}}\rvert < 1.5$, else $\lvert k_{\mathrm{dist}}\rvert < 0.5$ |
| 8 | SPFO | $p_{\mathrm{SPFO}} < 10$ GeV and $Q_{\mathrm{SPFO}} = Q_{\mathrm{LPFO}}$ |
| 9 | Charge | $Q_{\mathrm{LPFO}_1} \times Q_{\mathrm{LPFO}_2} < 0$ |

Table 1: Summary of the event selection cuts used in the baseline $dE/dx$ analysis.

significance quantifies the compatibility of a track with a given particle hypothesis, and it is defined as $S_{\mathrm{d}E/\mathrm{d}x} = \Delta(\mathrm{d}E/\mathrm{d}x)/\sigma_{\mathrm{d}E/\mathrm{d}x}$, where $\Delta(\mathrm{d}E/\mathrm{d}x) = (\mathrm{d}E/\mathrm{d}x)_{\mathrm{meas}} - (\mathrm{d}E/\mathrm{d}x)_{\mathrm{exp}}$. In this work, we take the Bethe-Bloch expectation for kaons as reference, which defines the $\mathrm{d}E/\mathrm{d}x$ *k-distance*, shown in Fig. 1.

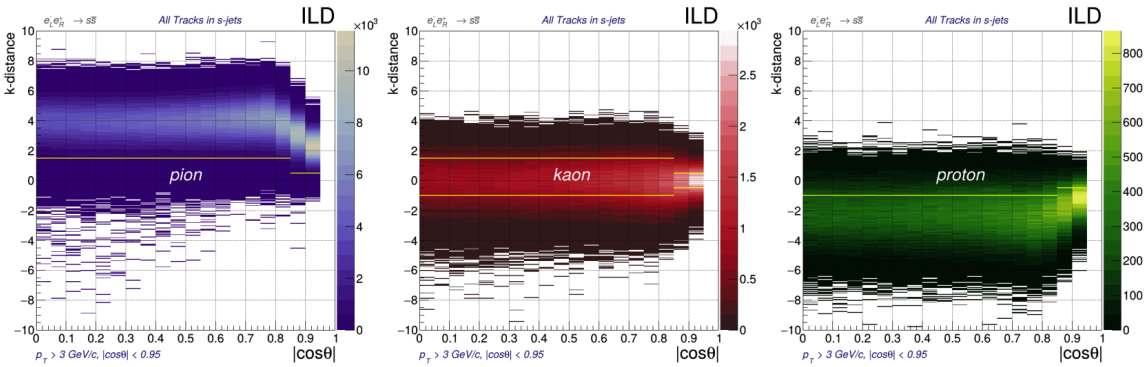


Figure 1: Kaon selection region in the $k$-distance plane used in cut 7.

The total and angular efficiencies for all quark flavours and for each $s$-tagging cut are reported in the Appendix.

For the $A_{FB}$ measurement, the jet charge is taken from the leading PFO, identified as a primary kaon from the $s$ or $\bar{s}$ quark. The selected sample is corrected sequentially: backgrounds are subtracted using templates scaled by their efficiencies, the signal is corrected for polar-angle-dependent selection and reconstruction efficiencies, and residual charge misidentification is corrected using the $p$–$q$ method.

### Template Subtraction and Efficiency Correction

Background contributions are estimated using truth-level Monte Carlo templates, scaled by the corresponding selection efficiencies $\varepsilon = N_{\mathrm{sel}}/N_{\mathrm{gen}}$ for each background $b$. The corrected signal yield in each bin is

$$N_{\mathrm{signal}} = N_{\mathrm{obs}} - \sum_b \varepsilon_b N_b, \tag{2}$$

after which, the signal is corrected for angular-dependent reconstruction and selection efficiency:

$$N_{\mathrm{corr}} = \frac{N_{\mathrm{signal}}}{\varepsilon_{signal}}. \tag{3}$$

### Migration Correction (p-q method)

Let $P_{\text{chg}}$ be the probability that the sign we infer from the LPFO correctly reproduces the charge of the initial quark produced in the hard scattering. The probability of misidentification is then $Q_{\text{chg}} = 1 - P_{\text{chg}}$. Assuming that the jet-charge measurements in the two hemispheres are independent and symmetric, the number of events with compatible charges (opposite sign) in a given $|\cos\theta|$ bin can be written as

$$N^{M}_{\text{acc}}(|\cos\theta|) = \left(P^2_{\text{chg}} + Q^2_{\text{chg}}\right) N(|\cos\theta|). \tag{4}$$

Once $P_{\text{chg}}$ is determined from Eq. 4, the observed events in the forward and backward regions can be unfolded to recover the true distributions. The corrected event yields are obtained by inverting the corresponding $2 \times 2$ migration system:

$$\begin{aligned} N_{\text{corr}}(+|\cos\theta|) &= \frac{P^2_{\text{chg}} N_{\text{acc}}(\cos\theta > 0) - Q^2_{\text{chg}} N_{\text{acc}}(\cos\theta < 0)}{P^4_{\text{chg}} - Q^4_{\text{chg}}}, \\ N_{\text{corr}}(-|\cos\theta|) &= \frac{P^2_{\text{chg}} N_{\text{acc}}(\cos\theta < 0) - Q^2_{\text{chg}} N_{\text{acc}}(\cos\theta > 0)}{P^4_{\text{chg}} - Q^4_{\text{chg}}}. \end{aligned} \tag{5}$$

This expression corresponds to the analytical inversion of the $2 \times 2$ charge-migration matrix under the assumption of identical charge-measurement performance in both jets.

### Fit

After applying the correction procedure, the resulting differential cross-section represents the parton-level distribution. This distribution is fitted using

$$\frac{d\sigma}{d\cos\theta} = S(1 + \cos^2\theta) + A\cos\theta, \tag{6}$$

neglecting the term proportional to $\sin^2\theta$, as it is strongly suppressed by the large Lorentz boost of the $s$-quarks. The fit is restricted to the barrel region, $|\cos\theta| < 0.8$, where the PFO information is not significantly affected by detector acceptance. The $A_{FB}$ value is obtained by extrapolating this function to the full angular range. This method is motivated by the reduced statistics and degraded reconstruction performance in the very forward/backward regions ($|\cos\theta| > 0.8$).

An example of these fits for the baseline $dE/dx$ case for $e^-_L e^+_R$ and $e^-_R e^+_L$ is shown in Fig. 2, comparing parton-level and reconstructed distributions for both polarizations.

## 3 Improvements in PID

### Software improvements

The same analysis as described in Sec. 2 was repeated using the *Comprehensive PID* (CPID) framework (Ref. [24]). In this approach, the particle identification for each PFO is based on the likelihood outputs of BDT classifiers. In particular, cut 7 was modified such that a PFO is considered a kaon if $L_K > 0.5$ and $L_\pi < 0.7$, where $L_{K/\pi}$ are the kaon/pion likelihood outputs of CPID. All other cuts are applied as in the $dE/dx$ analysis.

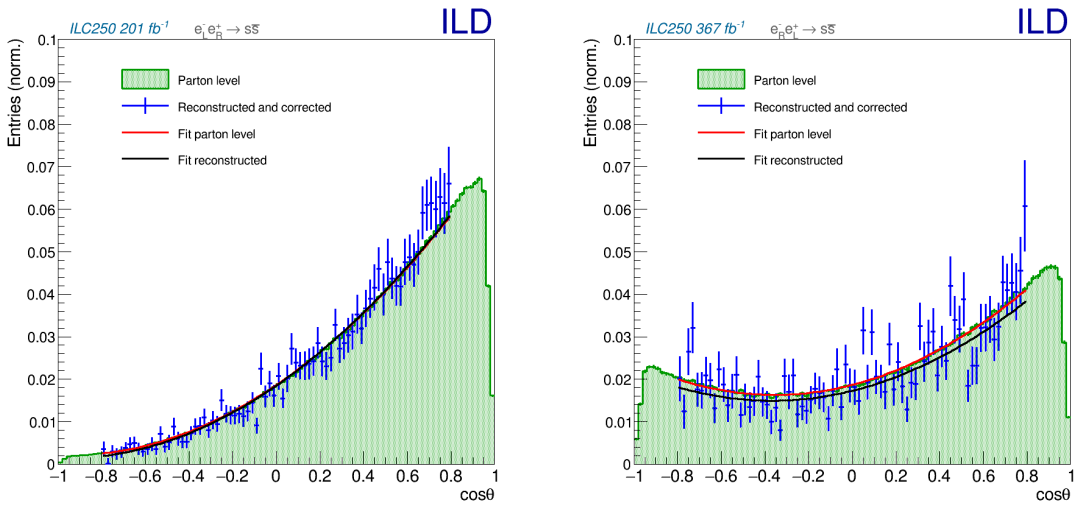


Figure 2: Comparison of the angular fits to the reconstructed and corrected data with respect to the parton level distributions. Plots for the $e_L^- e_R^+$ (left) and $e_R^- e_L^+$ (right) cases using $dE/dx$.

### Hardware improvements

Two scenarios are considered to evaluate the potential gain from improved PID. A pixel-based TPC is expected to improve kaon/pion separation by $\sim$ 30–40% for track momenta between 3 and 50 GeV [25] by using *Cluster Counting* ($dN/dx$). Since $dN/dx$ reconstruction is not yet available in ILD, its effect is emulated by narrowing the PID likelihood distributions, following Refs. [13, 15]. In the $dN/dx$ scenario, the standard deviation of the $k$-distance is reduced by 25% (corresponding to $\sim$ 33% improvement in separation), while in the *PerfectTPC* case it is reduced by 99%, representing near-ideal PID. The baseline $dE/dx$ analysis flow is applied in both cases for direct comparison.

## 4 Estimation of systematic uncertainties

Systematic uncertainties are evaluated by propagating the uncertainties on the selection efficiencies for both signal and background through the template subtraction procedure:

1. For each efficiency, variations are applied according to its uncertainty, generating pseudo-experiments (toys) in which efficiencies are fluctuated independently.

2. For each toy, the template subtraction is repeated, yielding a set of corrected signal distributions.

3. For each bin, the systematic uncertainty is computed as

$$\Delta = \sqrt{\Delta_{\text{disp}}^2 + \Delta_{\text{rms}}^2}, \tag{7}$$

   where $\Delta_{\text{disp}}$ is the mean shift of the toy results relative to the nominal value, and $\Delta_{\text{rms}}$ is the root-mean-square of the fluctuations around this mean.

This method naturally combines bias and spread in a single systematic uncertainty, and can account for correlations between bins if needed.

There are other sources of systematic uncertainties that haven't been considered here, such as polarization in the initial state or hemisphere correlation in the detector, but, as can be seen in Ref. [12], their size is minimal compared to the template subtraction.

## 5 Results for ILC250 and LCF@CERN250

Figures 3 and 4 summarise $A_{FB}$ results for ILC250 and LCF@CERN250. Statistical uncertainties are scaled to expected integrated luminosities. Improvements from CPID and hardware upgrades reduce uncertainties, with *PerfectTPC* providing a lower benchmark.

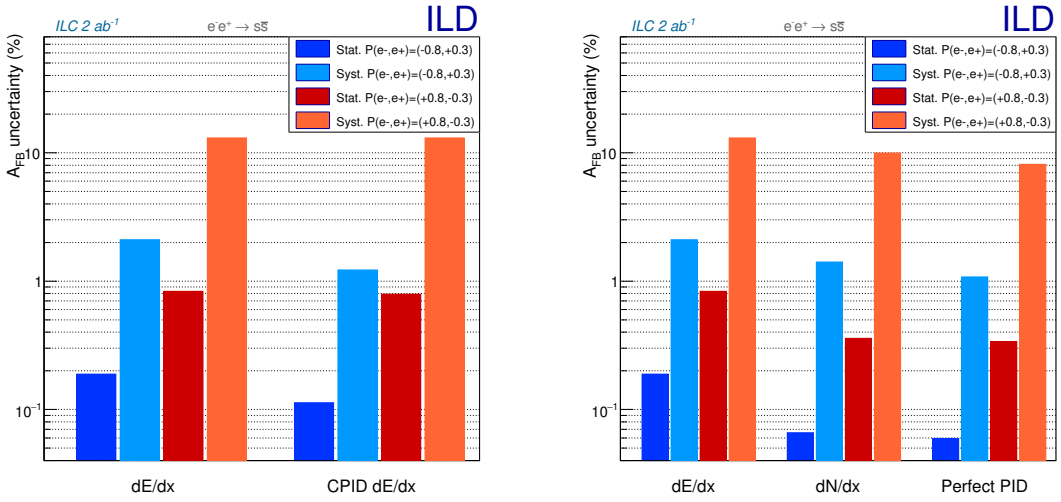


Figure 3: Expected uncertainties for $s\bar{s}$ in the ILC250. Right: Comparing different hardware settings ($dE/dx$ vs $dN/dx$ in a pixel TPC vs An ideal TPC)

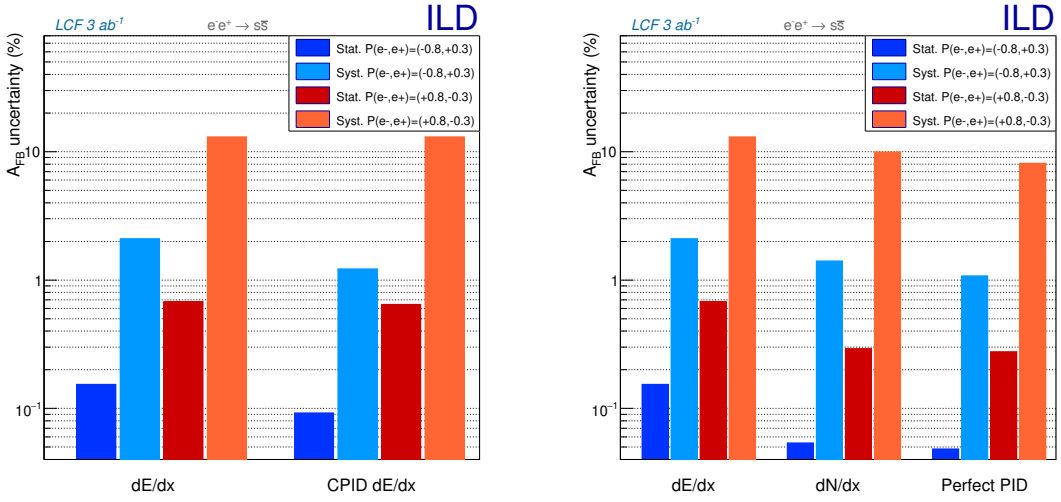


Figure 4: Expected uncertainties for $s\bar{s}$ in the LCF@CERN250. Left: Comparing different software approaches ($dE/dx$ vs CPID $dE/dx$). Right: Comparing different hardware settings ($dE/dx$ vs $dN/dx$ in a pixel TPC vs An ideal TPC)

## 6 Possible impact on GHU phenomenology

Figure 5 shows the potential impact of improved $s\bar{s}$ forward-backward asymmetry measurements on discriminating *Gauge-Higgs Unification* (GHU) scenarios. The plots follow the methodology of Ref. [15],

using projected experimental uncertainties from Ref. [26] as input. These uncertainties are indicative estimates for the $b\bar{b}$ and $c\bar{c}$ channels using the *Particle Transformer* (ParT); a dedicated analysis will be required. The figures demonstrate that even modest improvements in $s\bar{s}$ $A_{FB}$ can enhance sensitivity to GHU parameters.

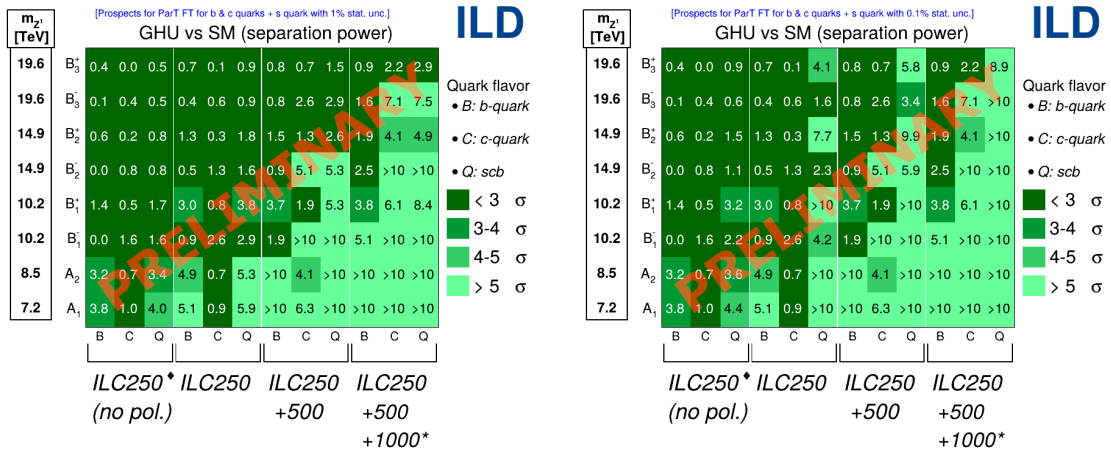


Figure 5: Expected impact in the discrimination power for GHU models assuming a 1% (left) or 0.1% (right) uncertainty for $s\bar{s}$.

## 7 Conclusions

This study highlights the improvements achievable in $s\bar{s}$ forward-backward asymmetry measurements using advanced particle identification. Upgrading from standard $dE/dx$ to emulated $dN/dx$ or applying CPID likelihood-based selection both reduce uncertainties and enhance the signal purity.

The results also illustrate the potential of this channel for probing BSM scenarios such as GHU. While the current cut-based approach provides a first estimate of the achievable precision, it does not fully exploit all available kinematic and PID information. Future studies using the ParT framework will allow more sophisticated selections, further improving sensitivity and maximizing the impact of this channel.

## Acknowledgements

We thank the LCC generator and ILD software working groups for supplying the simulation and reconstruction tools, as well as for producing the Monte Carlo samples employed in this study. We also thank A. Irles and Y. Okugawa for providing the software from the previous analyses, as well as very useful inputs for new developments.

## Appendix

### Efficiencies for the $dE/dx$ case

## References

[1] T. Behnke et al.,
*The International Linear Collider Technical Design Report - Volume 1: Executive Summary.* (2013), arXiv: 1306.6327 [physics.acc-ph].

| | Efficiency (%) | | | | |
|---|---|---|---|---|---|
| | dd | uu | ss | cc | bb |
| + Cut 1 | 93.9 | 93.9 | 93.1 | 69.3 | 2.11 |
| + Cut 2 | 91.8 | 91.6 | 90.9 | 14.0 | 1.35 |
| + Cut 3 | 91.8 | 91.6 | 90.9 | 14.0 | 1.35 |
| + Cut 4 | 44.9 | 51.8 | 42.3 | 4.01 | 0.07 |
| + Cut 5 | 38.2 | 43.9 | 35.9 | 3.35 | 0.06 |
| + Cut 6 | 36.8 | 42.4 | 34.0 | 3.10 | 0.05 |
| + Cut 7 | 2.38 | 2.91 | 4.80 | 0.22 | <0.01 |
| + Cut 8 | 0.29 | 0.46 | 0.63 | 0.04 | <0.01 |
| + Cut 9 | 0.17 | 0.33 | 0.48 | 0.02 | <0.01 |

Table 2: Efficiencies per cut in the $e_L^- e_R^+$ case.

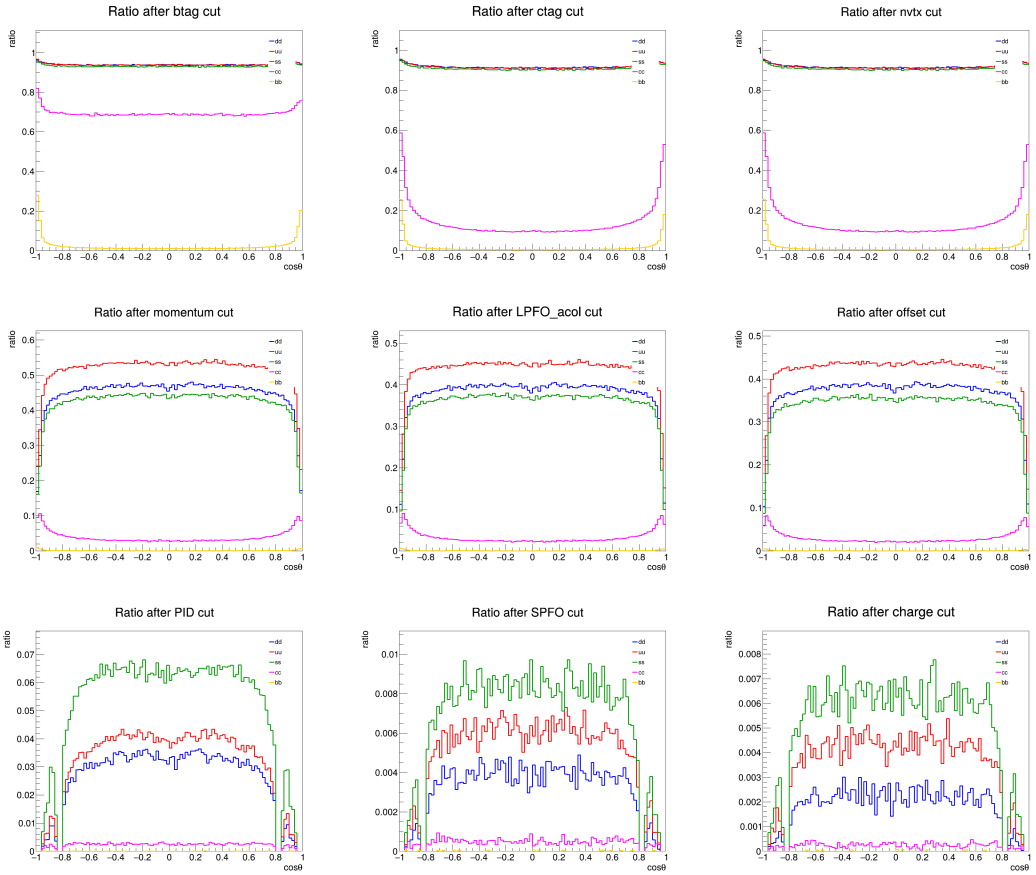


Figure 6: Efficiencies per cut in the $e_L^- e_R^+$ case.

[2] H. Baer et al., *The International Linear Collider Technical Design Report - Volume 2: Physics.* (2013), arXiv: 1306.6352 [hep-ph].

[3] C. Adolphsen et al., *The International Linear Collider Technical Design Report - Volume 3.I: Accelerator & in the Technical Design Phase.* (2013), arXiv: 1306.6353 [physics.acc-ph].

[4] C. Adolphsen et al., *The International Linear Collider Technical Design Report - Volume 3.II: Accelerator Baseline Design.* (2013), arXiv: 1306.6328 [physics.acc-ph].

| | Efficiency (%) | | | | |
|---|---|---|---|---|---|
| | dd | uu | ss | cc | bb |
| + Cut 1 | 94 | 93.9 | 93.2 | 69.3 | 3.45 |
| + Cut 2 | 92 | 91.7 | 91.1 | 14.6 | 2.46 |
| + Cut 3 | 92 | 91.7 | 91.1 | 14.6 | 2.46 |
| + Cut 4 | 38.2 | 50.4 | 35.9 | 3.92 | 0.07 |
| + Cut 5 | 32.4 | 42.7 | 30.4 | 3.30 | 0.06 |
| + Cut 6 | 31.3 | 41.2 | 28.8 | 3.04 | 0.05 |
| + Cut 7 | 1.99 | 2.84 | 4.07 | 0.22 | <0.01 |
| + Cut 8 | 0.26 | 0.44 | 0.53 | 0.04 | <0.01 |
| + Cut 9 | 0.15 | 0.32 | 0.40 | 0.02 | <0.01 |

Table 3: Efficiencies per cut in the $e^-_R e^+_L$ case.

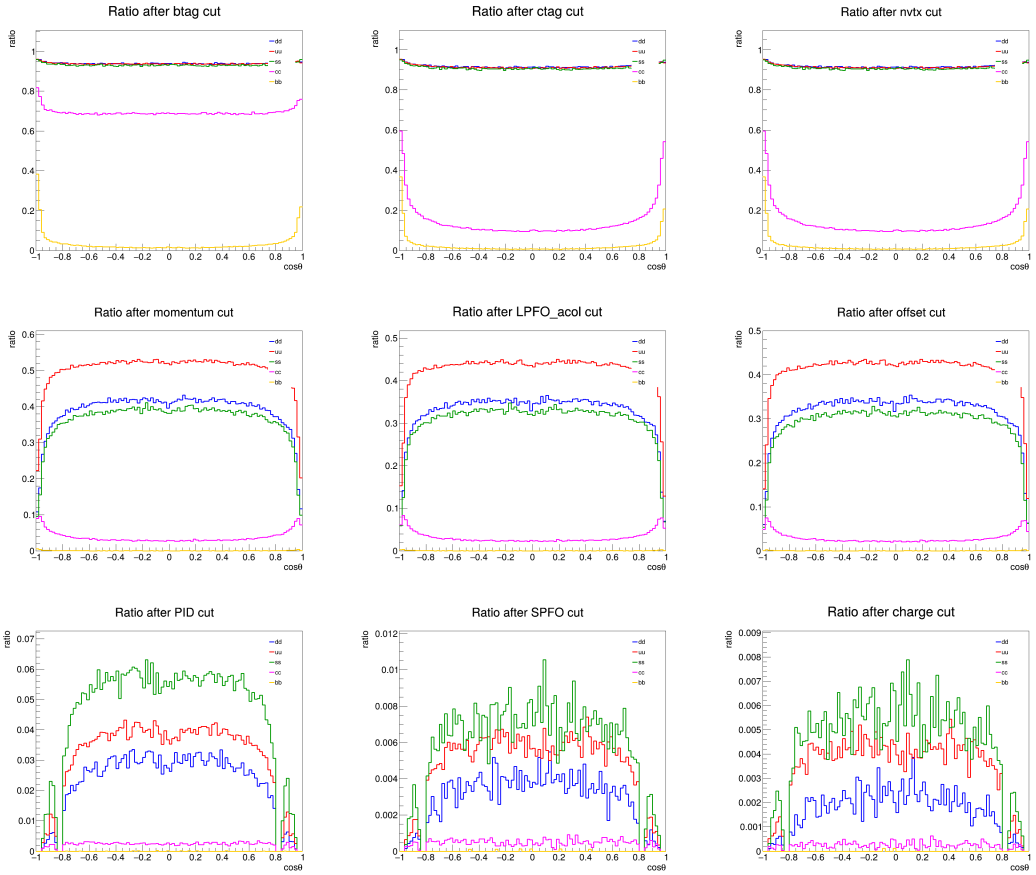


Figure 7: Efficiencies per cut in the $e^-_R e^+_L$ case.

[5] H. Abramowicz et al.,
*The International Linear Collider Technical Design Report - Volume 4: Detectors* (2013), ed. by T. Behnke et al., arXiv: 1306.6329 [physics.ins-det].

[6] H. Abramowicz et al., *The Linear Collider Facility (LCF) at CERN* (2025), arXiv: 2503.24049 [hep-ex].

[7] H. Abramowicz et al., *A Linear Collider Vision for the Future of Particle Physics* (2025), arXiv: 2503.19983 [hep-ex].

[8] A. Irles, R. Poeschl, F. Richard,
*Determination of the electroweak couplings of the 3rd generation of quarks at the ILC*,
PoS **EPS-HEP2019** (2020) 624, DOI: 10.22323/1.364.0624.

[9] Y. Okugawa et al., *Production and electroweak couplings of 3rd generation quarks at the ILC*,
PoS **LeptonPhoton2019** (2019) 170, DOI: 10.22323/1.367.0170.

[10] A. Irles, R. Poeschl, F. Richard,
*Production and measurement of $e^+e^- \to c\bar{c}$ signatures at the 250 GeV ILC*,
International Workshop on Future Linear Colliders (LCWS 2019) Sendai, Miyagi, Japan,
October 28–November 1, 2019, 2020, arXiv: 2002.05805 [hep-ex].

[11] A. Irles, J. P. Marquez, *Experimental prospects for precision observables in $e^-e^+ \to q\bar{q}$ with $q = b,c$ processes at the ILC operating at 250 and 500 GeV of center of mass*,
International Workshop on Future Linear Colliders, 2023, arXiv: 2307.14888 [hep-ex].

[12] A. Irles, R. Pöschl, F. Richard, *Experimental methods and prospects on the measurement of electroweak b and c-quark observables at the ILC operating at 250 GeV* (2023),
arXiv: 2306.11413 [hep-ex].

[13] J. P. Márquez, *Experimental prospects for indirect BSM searches in $e^+e^- \to q\bar{q}$ ($q = c,b$) processes at Higgs Factories.* PoS **EPS-HEP2023** (2024) 300,
DOI: 10.22323/1.449.0300, arXiv: 2310.17617 [hep-ph].

[14] Y. Okugawa, *Analysis of test beam data using a technological prototype of a highly granular calorimeter and study of light quark production at a future linear collider*, PhD thesis,
Laboratoire de Physique des 2 Infinis Irène Joliot-Curie, France, U. Paris-Saclay, 2024.

[15] A. Irles et al., *Probing gauge-Higgs unification models at the ILC with quark–antiquark forward–backward asymmetry at center-of-mass energies above the Z mass*,
Eur. Phys. J. C **84** 5 (2024) 537, DOI: 10.1140/epjc/s10052-024-12918-z,
arXiv: 2403.09144 [hep-ph].

[16] Y. Okugawa et al.,
*Quark production in high energy electron positron collisions: from strange to top*,
PoS **ICHEP2022** (2022) 871, DOI: 10.22323/1.414.0871.

[17] W. Kilian, T. Ohl, J. Reuter, *WHIZARD: Simulating Multi-Particle Processes at LHC and ILC*,
Eur. Phys. J. **C71** (2011) 1742, DOI: 10.1140/epjc/s10052-011-1742-y,
arXiv: 0708.4233 [hep-ph].

[18] M. Frank et al., *DD4hep: A Detector Description Toolkit for High Energy Physics Experiments*,
J. Phys. Conf. Ser. **513** (2014), ed. by D. L. Groep, D. Bonacorsi 022010,
DOI: 10.1088/1742-6596/513/2/022010.

[19] D. Schulte, *Beam-beam simulations with GUINEA-PIG* (1999).

[20] T. Sjöstrand, S. Mrenna, P. Skands, *PYTHIA 6.4 physics and manual*,
Journal of High Energy Physics **2006** 05 (2006) 026,
DOI: 10.1088/1126-6708/2006/05/026.

[21] M. Thomson, *Particle flow calorimetry and the PandoraPFA algorithm*,
Nuclear Instruments and Methods in Physics Research Section A: Accelerators, Spectrometers, Detectors and Associated Equipment **611** 1 (2009) 25–40, ISSN: 0168-9002,
DOI: 10.1016/j.nima.2009.09.009,
URL: http://dx.doi.org/10.1016/j.nima.2009.09.009.

[22] T. Suehara, T. Tanabe, *LCFIPlus: A Framework for Jet Analysis in Linear Collider Studies*,
Nucl. Instrum. Meth. A **808** (2016) 109, DOI: 10.1016/j.nima.2015.11.054,
arXiv: 1506.08371 [physics.ins-det].

[23] H. Abramowicz et al., *International Large Detector: Interim Design Report* (2020), arXiv: 2003.01116 [physics.ins-det].

[24] U. Einhaus, *CPID: A Comprehensive Particle Identification Framework for Future $e^+e^-$ Colliders* (2023), arXiv: 2307.15635 [hep-ex].

[25] Y. Aoki et al., *Double-hit separation and dE/dx resolution of a time projection chamber with GEM readout*, JINST **17** 11 (2022) P11027, DOI: 10.1088/1748-0221/17/11/P11027, arXiv: 2205.12160 [physics.ins-det].

[26] J. Altmann et al., *ECFA Higgs, electroweak, and top Factory Study*, vol. 5/2025, CERN Yellow Reports: Monographs, 2025, ISBN: 978-92-9083-700-8, 978-92-9083-701-5, DOI: 10.23731/CYRM-2025-005, arXiv: 2506.15390 [hep-ex].